Chapter II

Singlet Fission in Coordination Complexes of Dipyridyl Pyrrole Bipentacenes

Introduction

Singlet fission is a multiexciton generating (MEG) process in organic chromophores by which a photon promotes electronic excitation to a singlet exciton that can then relax into a pair of triplet excitons. This pair of triplets is initially generated as an overall spin-correlated singlet state, and, often when in solid media, these triplets can diffuse and thermalize into individual excitons via Dexter-type triplet energy transfer. Thus, singlet fission is spin-allowed and can occur on ultrafast timescales in contrast to traditional intersystem crossing from the singlet to triplet manifold, which is typically slow in the absence of strong spin-orbit coupling.[1,2]

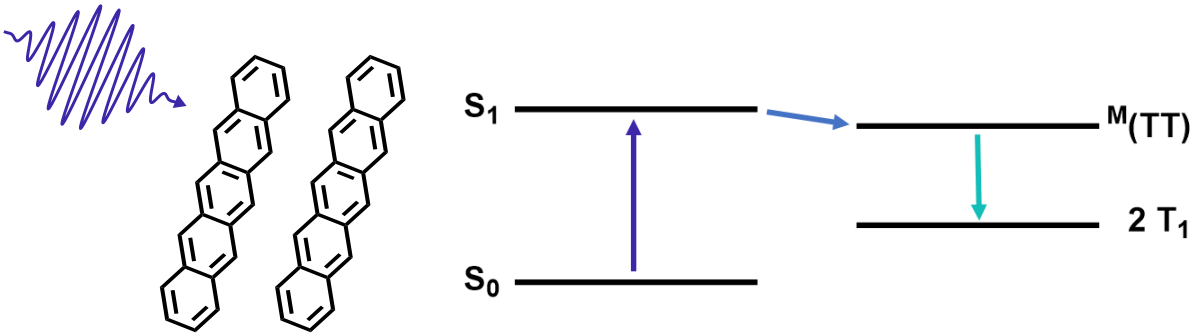

Figure 2.1 A schematic of singlet fission in a simplified Jablonski diagram and a depiction of a pair of pentacene molecules being excited by a photon.

Although singlet fission was first elucidated in the 1960s, the field was reinvigorated with the observation that MEG processes could be employed to surpass the Shockley-Quiesser efficiency limit of single-junction solar cells (~30%) to nearly 40%. A significant source of efficiency loss in solar cells is a result of thermalization of absorbed photon energy to the semiconductor band edge, which generally occurs on timescales faster than charge separation. As such, much of the energy imparted by the higher-energy portion of the solar spectrum is lost

thermally and is not converted into electrical energy. Higher efficiencies can be achieved in multijunction cells where semiconductor materials with varying bandgaps are layered such that each can most efficiently convert a different portion of the solar spectrum. However, such multijunction cells are often costly to make and may not be amenable to mass production.[3–8]

Singlet fission provides a competitive path to downconvert high-energy photons into lower energy (triplet) excitons that may be efficiently converted into photocurrent by a traditional semiconductor material, circumventing a portion of the thermalization loss. Singlet fission-based organic photovoltaics have even been realized with external quantum efficiencies exceeding 100% in pentacene/C60 junctions.[9–11]

In addition to the possibility of solar cell applications, singlet fission has also garnered attention for possible implications in quantum information science. The multiexcitonic state represents a maximally entangled state that can be described as a strong correlation between individual triplet excitons. Studies have suggested that the spin correlations in such states can persist out to μm scales in solid-state systems.[12–20]

Despite the possibilities offered by singlet fission, there remain challenges to realizing the potential of such systems. First, the range of chromophores that can demonstrate singlet fission is limited due to the energetic requirements. For the generation of two triplets from an excited singlet to be efficient, the adiabatic energy of the singlet excited state must be roughly twice the energy of the triplet such that energy is conserved in the transition (i.e. $E_{S_1} \approx 2E_{T_1}$). Second, the utility of singlet fission rests in the electronic structure of the triplet pair state, which is still not well understood. For example, strong interchromophore coupling may engender fast and efficient transfer from the singlet exciton to the triplet pair state, but may also hinder triplet separation, posing a challenge for efficient charge extraction, although there is a suggestion that the triplet

pair state may enable multielectron transfer at heterojunction interfaces. The persistence of spin correlation in the triplet pair state is also necessary for applications in quantum information science. Thus, in addition to the elucidation of novel chromophores for singlet fission, a deeper understanding of the electronic structure and dynamics that govern this process may aid in the engineering of singlet fission devices.[1]

Covalently linked chromophore dimers represent a way to control excitonic interactions using synthetically-tuned molecular scaffolds. Molecular bipentacenes, for example, have become an important tool for the study of singlet fission.[21–23] Singlet fission is exergonic and highly efficient in pentacene systems.[1,24,25] Much focus has been given to the nature of the synthetic linker on rates and efficiencies of singlet fission. For example, bipentacenes linked by a phenyl moiety can be perturbed by examining the *ortho*-, *meta*-, or *para*- configurations.[26] Oligophenyl linkers have been explored, extending the distance between pentacene moieties by increasing the number of intervening phenyl rings.[27] In addition to conjugated linkers, aliphatic groups have been explored to attenuate the through-bound coupling between pentacene rings.[28] Such studies have elucidated the importance of interchromophore coupling, Davydov splitting in molecular excited states, and have also permitted the observation of multiexcitonic quintet states by time-resolved electron paramagnetic resonance (TREPR) spectroscopy.[14,28–30]

Varying the covalent linker in these bipentacene systems has proven to be a versatile approach toward addressing fundamental aspects of SF.[31–41] However, disentangling the contributions of through-bond and through-space effects that give rise to the properties of a given system remain a challenge. In our studies, we have sought to study synthetic bipentacene systems covalently linked by ligand scaffolds capable of binding metal ions. In this way, we can examine

how a singular molecular bipentacene framework can give rise to tunable singlet fission by means of coordination-induced structural changes.

In our initial study, we synthesized and characterized the photophysics of a dipyridyl pyrrole-linked bipentacene (HDPP-Pent). We were able to deprotonate HDPP-Pent and form complexes with lithium and potassium cations forming Li_2(DPP-Pent)$_2$ and KDPP-Pent, a solution-state dimer and monomer structure respectively. These complexes maintain the same backbone linking the pentacene rings together while modulating the arrangement and interaction of the pentacenes and thus influence the rate of singlet fission. This series provides new ideas for the control of singlet fission via dimer self-assembly promoted by metal coordination.

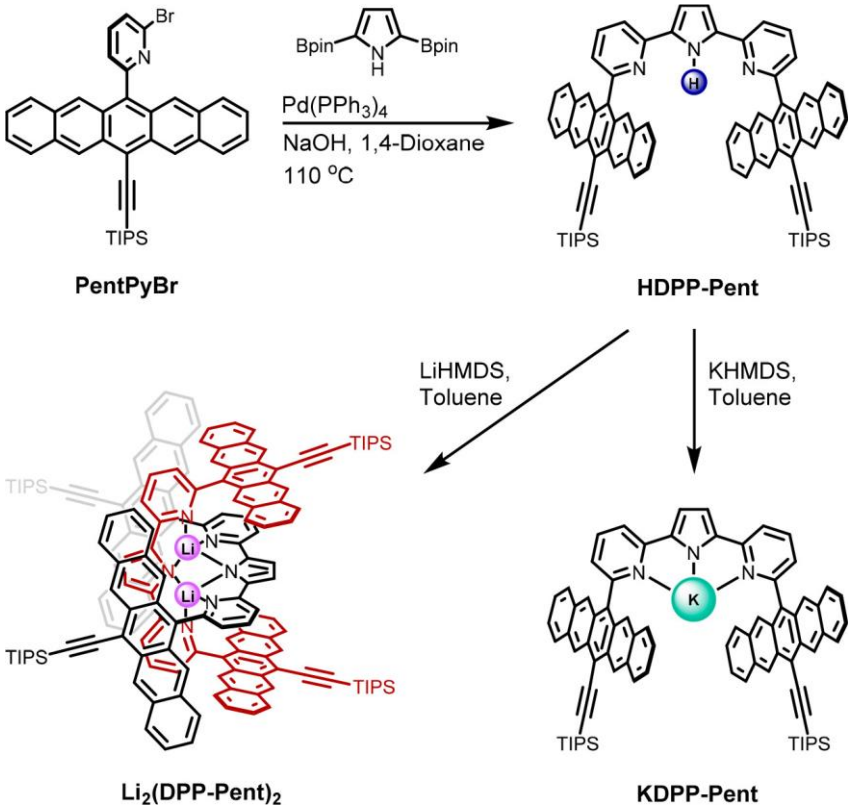

Figure 2.2 Synthesis of HDPP-Pent and MDPP-Pent complexes.

Synthesis and NMR Characterization

HDPP-Pent was synthesized from a monopentacene pyridyl bromide derivative PentPyBr, which we employ as a monopentacene reference compound in our optical spectroscopic studies. The ^{1}H NMR spectrum of HDPP-Pent is broad in the aromatic region, in contrast to the well-resolved scalar coupling between protons on the terminal rings of the pentacene moiety observed for PentPyBr. Variable temperature ^{1}H NMR from 20 to -80 °C reveals complex temperature-dependent behavior. The aromatic region broadens further cooling to -40 °C, and many new resonances grow in with further cooling.

HDPP-Pent serves as a ligand by protonolysis of the pyrrole N-H bond. Using a strong amide base such as lithium or potassium hexamethyldisilazide provides formation of Li_2(DPP-Pent)$_2$ or KDPP-Pent, respectively. Despite the broad features of the HDPP-Pent ^{1}H NMR spectrum, deprotonation leads to sharp and well-resolved spectra for the alkali metal complexes at room temperature. In comparison to the ^{1}H NMR spectrum of KDPP-Pent, it is evident that the protons on the dipyridyl pyrrolide moiety of Li_2(DPP-Pent)$_2$ are significantly upfield shifted. The singlet resonance corresponding to the pyrrolide ring proton is found at 4.38 and 7.03 ppm in the Li_2(DPP-Pent)$_2$ and KDPP-Pent spectra, respectively.

We carried out 2D rotating frame Overhauser enhancement spectroscopy (ROESY) on Li_2(DPP-Pent)$_2$, which showed through space ^{1}H-^{1}H coupling between protons on the dipyridyl pyrrolide backbone at 4.38 ppm (H_c) and 5.14 ppm (H_d) and the proton on the distal side of the pentacene ring at 9.12 ppm (H_a) (denoted by green and blue circles, respectively, in Figure 2.3B). No such cross-peaks are observed in the 2D ROESY spectrum of KDPP-Pent (Figure 2.3C). More information regarding the choice of 2D ROESY vs. 2D NOESY can be found in Appendix A.

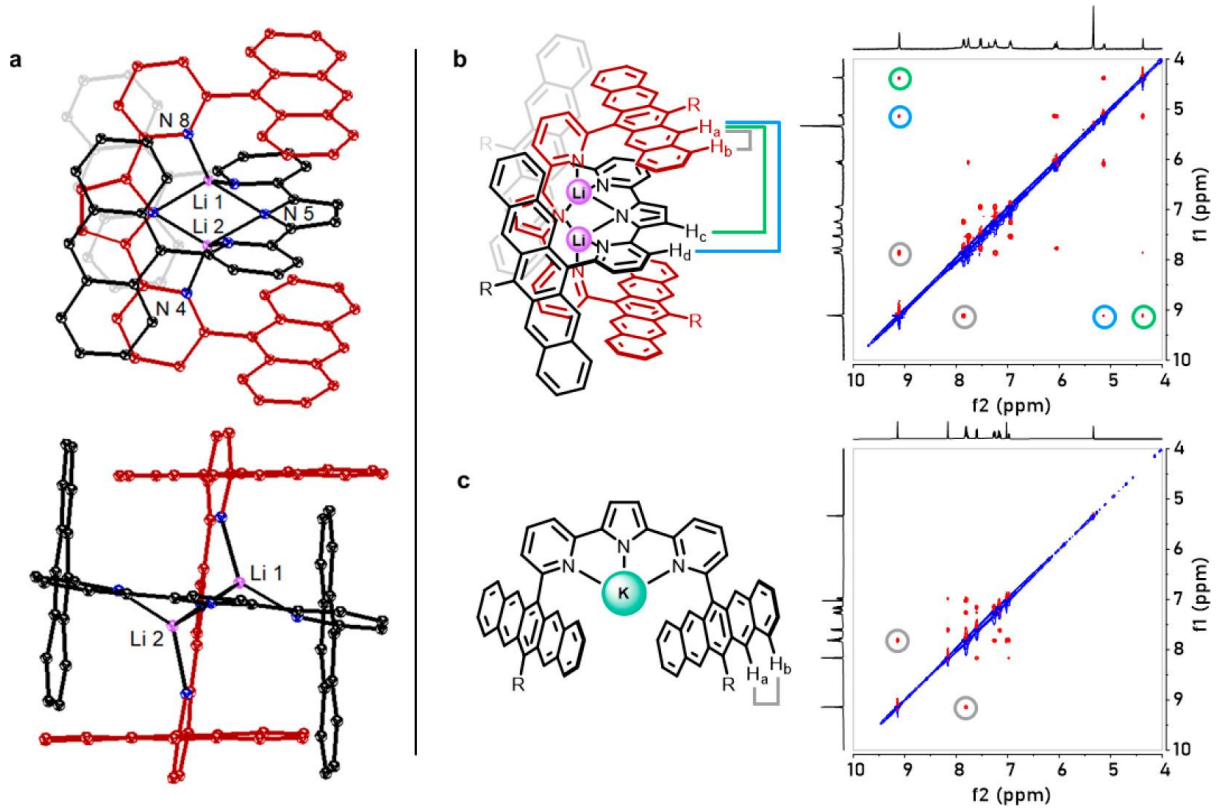

Figure 2.3 Structural data supporting dimeric $Li_2(DPP\text{-}Pent)_2$ and monomeric KDPP-Pent assignments in solution. (**A**) Crystallographic identification of a dimeric Li complex with an analogous ligand, DPP-Anth, in two perspectives, (**B**) proposed dimeric structure of $Li_2(DPP\text{-}Pent)_2$ and the corresponding through-space coupling highlighted in the respective 2D-ROESY spectrum, and (**C**) proposed monomeric structure of KDPP-Pent and the corresponding through-space coupling highlighted in the respective 2D-ROESY spectrum; R = triisopropylsilylethynyl.

Analysis of NMR Data

We interpret the broadness of the room temperature ^{1}NMR spectrum of HDPP-Pent as being due to conformational dynamics. Such dynamics may involve rotations around aryl-aryl linkages resulting in mixtures of conformers that interconvert on an intermediate timescale on the

order of the NMR experiment. The variable temperature data suggests this as well, although the complexity of this dataset occludes further interpretation. The multitude of resonances observed at -80 °C may result from a freezing out of multiple solution-state structures, monomeric or dimeric. The aromatic features are resolved upon deprotonation and metal coordination of the DPP-Pent framework as evidenced by the sharp spectra observed for Li_2(DPP-Pent)$_2$ and KDPP-Pent, suggesting the formation of single solution-state conformers or fast exchange processes.

The NMR data collected on Li_2DPP-Pent$_2$ strongly suggest a dimeric solution-state structure as proposed in Figure 2.B. The π-stacking interactions between the pentacene and sandwiched dipyridyl pyrrole units are consistent with the upfield shift exhibited by the dipyridyl pyrrole protons owing to enhanced chemical shielding by perturbation of the aromatic ring currents.[42,43] The cross-peaks in the 2D-ROESY spectrum between the pyrrole backbone protons and the protons on the far side of the pentacene also support a dimeric structure. The dipolar couplings that give rise to ROE are sensitive generally out to 5 Å, and this dimeric structure would bring the relevant nuclei into proximity for this interaction.[44,45] The spectra in Figure 2.3 were taken in CD_2Cl_2 to unambiguously assign the transitions observed in the aromatic region. Notably, the upfield shift and 2D ROESY cross-peaks are reproduced in toluene-*d8*. This suggests that the same dimeric structure is present in toluene, which we use for our transient optical measurements.

X-Ray quality single crystals of the pentacene derivatives have eluded us, but we have been able to crystallographically characterize a related lithium dipyridyl pyrrolide with anthracenyl moieties in place of the pentacenyl substituents, Li_2(DPP-Anth)$_2$ (Figure 2.3A). The structure of Li_2(DPP-Anth)$_2$ illustrates the formation of a dimeric species with two Li cations bridged by pyrrolide donors. We propose that Li_2(DPP-Pent)$_2$ has a similar geometry in solution.

The NMR data collected for KDPP-Pent stand in contrast to those of Li_2(DPP-Pent)$_2$. For KDPP-Pent, the dipyridyl pyrrole backbone protons do not display a significant upfield shift or observable cross-peaks between pyrrole and distal pentacene protons in the 2D ROESY spectrum. Therefore, we conclude that KDPP-Pent exists as a monomeric species in solution. We postulate that the small ionic radius of Li^+ permits dimer formation along with favorable π-π interactions, whereas the larger size of K^+ destabilizes such a structure.

Steady-State Absorption and Emission

The steady-state absorption spectra of PentPyBr, HDPP-Pent, Li_2(DPP-Pent)$_2$, and KDPP-Pent in toluene are compared in Figure 2.4A. As with most pentacene derivatives, the $S_1 \leftarrow S_0$ absorption band is observed with pronounced vibronic progression in the 500 – 650 nm region for all four compounds. A weaker vibronically structured band associated with the $S_2 \leftarrow S_0$ pentacene transition can also be observed in all spectra in the 400 – 450 nm region. Notably, the $S_1 \leftarrow S_0$ absorption in HDPP-Pent is roughly twice the intensity of that in PentPyBr with relatively little difference in peak positions (the λ_{max} of the $S_1 \leftarrow S_0$ 0-0 transition is at 622 nm in both spectra). As well, the relative intensities of the vibronic bands within the $S_1 \leftarrow S_0$ electronic transitions are relatively unchanged between HDPP-Pent and PentPyBr. The $S_1 \leftarrow S_0$ band in Li_2(DPP-pent)$_2$ is slightly broadened and the 0-0 band is modestly red-shifted by 5 nm (~130 cm^{-1}) from that of HDPP-Pent. Additionally, both Li_2(DPP-Pent)$_2$ and KDPP-Pent exhibit enhanced absorption intensity near 400 – 500 nm.

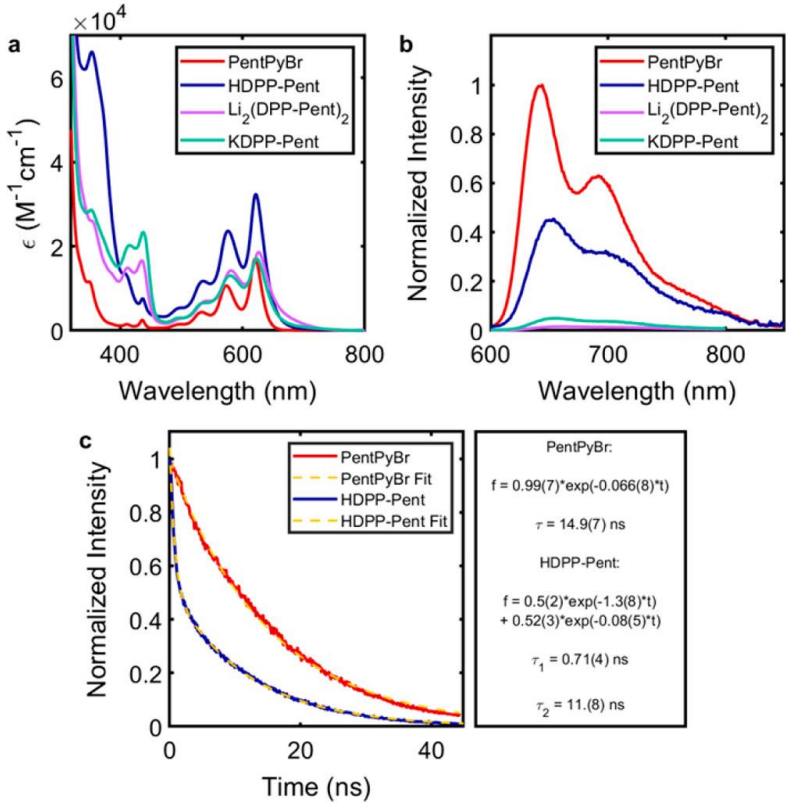

Figure 2.4 Steady-state absorption and emission spectra and time-resolved luminescence data of the pentacene series. Shown are the (**A**) absorption spectra; (**B**) the normalized emission spectra of PentPyBr (red), HDPP-Pent (blue), $Li_2(DPP\text{-}Pent)_2$ (purple), and KDPP-Pent (green) in toluene solutions; and (**C**) time-resolved luminescence traces and fits for PentPyBr (20 μM, toluene) and HDPP-Pent (20 μM, toluene). Note that the steady-state emission spectra are normalized by their relative integrated emission intensities.

Steady-state emission spectra for PentPyBr and HDPP-Pent are compared in Figure 2.4B. Here, the 0-0 emission band of HDPP-Pent (λ_{max} = 650 nm, ~ 15,400 cm^{-1}) is red-shifted from that of PentPyBr (λ_{max} = 640 nm, ~15,600 cm^{-1}) and broadened. The emission observed in this region is consistent with the $S_1 \rightarrow S_0$ fluorescence observed in related pentacene compounds.[46] We found the fluorescence quantum yield of PentPyBr in toluene to be 0.75, comparable to that reported for

TIPS-Pentacene. We found the fluorescence quantum yield of HDPP-Pent to be 0.43, significantly decreased in comparison to the single pentacene in PentPyBr. While Li_2(DPP-Pent)$_2$ and KDPP-Pent display similar emission profiles to HDPP-Pent, the integrated emission intensity is significantly reduced relative to HDPP-Pent.

Time-Resolved Luminescence

We collected time-resolved luminescence traces near the λ_{max} of the 0-0 emission band for PentPyBr (640 nm) and HDPP-Pent (650 nm) as shown in Figure 2.4C. The fluorescence decay for PentPyBr fits well to a monoexponential with a lifetime of ~15 ns. The fluorescence decay for HDPP-Pent, however, must be fit with a biexponential function with a first time constant of 0.71(4) ns and a second of 11.(8) ns. The latter of these two time constants is more consistent with the intrinsic fluorescence decay of the pentacene unit as observed in PentPyBr.

Emission Analysis

For efficient singlet fission (i.e. triplet yields approaching 200%), we expect the prompt fluorescence intensity to vanish, as the fission pathway must deplete the excited S_1 state more efficiently than emission. When singlet fission is sufficiently exothermic, which is the case for pentacene, the reverse triplet-triplet upconversion (fusion) becomes unfavorable, excluding delayed fluorescence. The observation of steady-state fluorescence intensity in HDPP-Pent already indicates that if singlet fission is occurring in this system, it is not operating at full efficiency. Nevertheless, the reduced fluorescence quantum yield of HDPP-Pent relative to PentPyBr suggests that a new, nonemissive relaxation pathway associated with the 0.71(4) ns time constant from the time-resolved luminescence experiment is present in the bipentacene that is not observed in the monopentacene. The biexponential decay of the luminescence signal also suggests that there may

be heterogeneous populations of HDPP-Pent that are excited in the process. For example, different conformers of HDPP-Pent may give rise to efficient pentacene-based emission, whereas others promote the faster nonradiative pathway.

Transient Absorption Spectroscopy – HDPP-Pent

To provide deeper insight into the nature of the nonradiative relaxation process in HDPP-Pent, we performed femtosecond transient absorption (fsTA) spectroscopy on PentPyBr and HDPP-Pent. The fsTA data of PentPyBr (Appendix A, Figure A.14) reveal a single major excited state absorption (ESA) with a λ_{max} around 450 nm (~22,200 cm^{-1}), which is consistent with previous assignments of absorption within the singlet excited state manifold (^{1}ESA) of related pentacene compounds. The observed ^{1}ESA decays monoexponentially over the time window, consistent with the time-resolved fluorescence data.

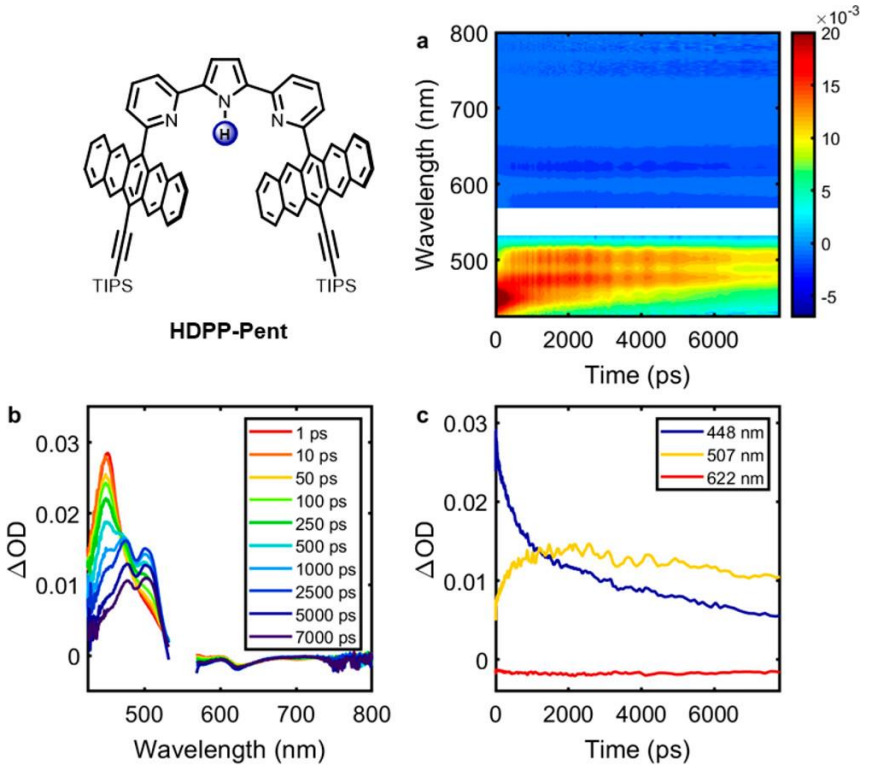

Figure 2.5 Visible transient absorption spectra—HDPP-Pent. The visible femtosecond transient absorption spectra of HDPP-Pent (50 μM, toluene) after excitation at 550 nm (0.100 μJ/pulse) are depicted: (**A**) contour plot, (**B**) spectral traces at various time delays, and (**C**) selected time traces at 448, 507, and 622 nm.

The fsTA data for HDPP-Pent are given in Figure 2.5. A ^{1}ESA at 450 nm is observed at early time delays, but it decays across the fsTA spectrum with the concomitant rise of a new, vibronically structured ESA with a λ_{max} = 510 nm (~19,600 cm^{-1}). This new ESA is consistent with previous literature reports that assign this band to transitions arising from triplet states pentacene (^{3}ESA). It is notable that in these prior reports, there is often little distinguishing the triplet pair excited state from an uncoupled triplet in the visible portion of the TA spectrum. In support of this assignment, we carried out photosensitization experiments in which binary mixtures of anthracene and HDPP-Pent are excited at 360 nm. At this wavelength, anthracene is preferentially excited at the given concentrations, undergoes intersystem crossing, and subsequently can undergo triplet-triplet energy transfer with HDPP-Pent as a means of independently preparing the free triplet state on HDPP-Pent. The long-lived triplet spectrum of HDPP-Pent acquired in these photosensitization experiments corresponds directly to the long-lived species observed in the direct excitation experiments (ESA λ_{max} = 510 nm), corroborating our assignment of this feature as a ^{3}ESA. This triplet signal is not appreciably observed for PentPyBr. The nanosecond TA (nsTA) data for HDPP-Pent (Appendix A, Figure A.10) reveal the decay of triplet signal back to baseline. Comparing the TA data of PentPyBr and HDPP-Pent suggests that the nonradiative pathway in HDPP-Pent may be associated with a transition from the S_1 to the T_1 or ^{M}(TT) states, as indicated by rise of the prominent ^{3}ESA feature with the correlated decay of the ^{1}ESA feature.

Kinetic Modeling

Kinetic modeling was carried out using global and target kinetic analysis on an interpolated dataset of the fsTA and nsTA spectra of HDPP-Pent in order to capture the complete relaxation dynamics. Using target analysis, the entire TA dataset is fitted over all wavelengths and all time delays with the application of a kinetic model. The preparation of the composite dataset and full description of the model applied to HDPP-Pent is provided in Appendix A along with fits for the individual fsTA and nsTA spectra for reference.

The results of our time-resolved luminescence data were used to inform our TA modeling as an independent probe of the S_1 dynamics, leading to a four-component model in which components 1 and 2 equally reflect the ^{1}ESA spectrum, and components 3 and 4 represent the ^{3}ESA spectrum. Component 1 decays into components 3 and 4 equally with a rate constant k_1; component 2 decays to the ground state with rate constant k_2; and components 3 and 4 decay to the ground state decay with rate constants k_3 and k_4, respectively.

This model was applied in two cases: one in which k_1 and k_2 were allowed to vary freely, and one in which k_1 and k_2 were fixed to 1.4 and 0.08 ns^{-1}, respectively, as obtained directly from the time-resolved fluorescence fits. The results of the free and fixed fittings are shown in Appendix Tables A.1 and A.2, respectively. Of note, the results for k_1, k_3, and k_4 are remarkably consistent between the two fits. Even when allowed to vary, the fit of k_1 gives a time constant $\tau_1$of 0.74(6) ns, consistent with the $\tau \sim 0.71$ ns obtained from emission data. This k_1 corresponds to the nonradiative transition from S_1 to T_1 within our model. k_2 shows the largest divergence in the two fits: τ_2 = 4.9(5) ns when allowed to vary from the fixed value of 11.(8) ns. Both values are consistent with the fluorescence lifetime, though error may come from the overlapping of spectral features in the combined fs/nsTA data.

Triplet Yield Estimation – HDPP-Pent

We estimated the triplet yield after direct excitation of HDPP-Pent from the transient absorption data and kinetic modeling. First, the extinction coefficient of the HDPP-Pent triplet absorption spectrum at 510 nm was determined via the triplet energy transfer method using anthracene as a triplet donor under pseudo-first-order kinetic conditions.[47–49] The extinction coefficient of the anthracene triplet spectrum at has previously been reported in toluene.[49] From this, we approximate the extinction coefficient of the HDPP-Pent triplet spectrum at 510 nm to be roughly 49,000 M^{-1} cm^{-1}.

We must be cautious in directly applying the Beer-Lambert law to estimate the concentration of photogenerated triplets in the TA spectrum of HDPP-Pent. Comparing early time traces of the fsTA spectrum where the singlet spectrum dominates to later time traces dominated by the triplet features, it is evident that the ^{1}ESA has spectral intensity at 510 nm that overlaps with the ^{3}ESA feature. As we know from the time-resolved luminescence data, there should be population of the singlet excited state of HDPP-Pent throughout the time scale of the fsTA spectrum owing to the contributions associated with the 11.(8) ns time constant. This means that even when the triplet spectrum at 510 nm reaches its maximum ΔOD intensity, there may be nonnegligible contribution to that signal from the other population of singlet excited HDPP-Pent.

As is shown explicitly in Appendix A, the target model can be used to decompose the maximum ΔOD into its contributions from the ^{1}ESA and ^{3}ESA as 2.8 and 10.0 mOD respectively, using the species associated spectra (SAS) and corresponding concentration profiles. Therefore, after direct excitation of HDPP-Pent in toluene solution, the value of 10.0 mOD for the effective ^{3}ESA intensity provides an estimated triplet yield of ~100%.

Analysis of Singlet Fission in HDPP-Pent

Comparison of the steady-state and time-resolved emission data for HDPP-Pent and PentPyBr indicates that there is at least a population of excited HDPP-Pent molecules that undergo a faster nonradiative relaxation process that is not significant in the monopentacene reference. We collected fs/nsTA data for both samples to further examine this pathway. In HDPP-Pent, the decay of the ^{1}ESA gave rise to significant ^{3}ESA intensity, whereas in PentPyBr, only the decay of the ^{1}ESA was observed. The HDPP-Pent data were modeled given a kinetic scheme in which two populations of HDPP-Pent S_1 state are present and they decay in diverging pathways. This supports the assignment of the fast relaxation time observed in the time-resolved luminescence to be associated with singlet to triplet conversion.

Finally, the triplet yield of HDPP-Pent is estimated to be 100% out of a maximum 200%. As previously noted, the fluorescence quantum yield of HDPP-Pent is 43%. The weighting coefficients of the exponential decays observed in the time-resolved luminescence data are also ~0.5 each. Taken together, these data are self-consistent with a model in which nearly half of the photogenerated singlets give rise to double the number of triplets. We therefore assign the nonradiative transition in HDPP-Pent as intramolecular singlet fission.

Li_2(DPP-Pent)$_2$ and KDPP-Pent

The HDPP-Pent analysis provides a foundation to understand the dynamics exhibited by the alkali metal complexes. The fsTA data for Li_2(DPP-Pent)$_2$ are shown in Figure 2.6. At early time delays, there is a ^{1}ESA feature with a λ_{max} at 450 nm that decays and gives rise to a strong ^{3}ESA centered at 515 nm (~19,400 cm^{-1}). The composite fs/nsTA data of Li_2(DPP-Pent)$_2$ can be kinetically modeled with either a three- or four-component model. In the three-component model,

the S_1 state is converted into the triplet manifold with a time constant τ_1 = 96.(2) ps; the triplet feature is fitted to a biexponential decay with time constants τ_2 = 23.(3) ns and τ_3 = 35.(0) μs. In the four-component model, the S_1 state is converted to the triplet manifold with a time constant τ_1 = 0.11(1) ns, and the triplet feature is fitted to a triexponential decay (τ_2 = 10.(7) ns, τ_3 = 0.1(3) μs, and τ_4 = 50.(1) μs).

Biexponential decays observed for the triplet features are not uncommon in the transient absorption spectra of fission-active bipentacenes. The two decay components are typically ascribed to geminate triplet pair recombination and free/decorrelated triplet decay processes (the former typically on the faster timescale than the latter). Triexponential triplet decays have also been fitted in the singlet fission literature. Notably, this is seen in related adamantane-derived bi- and tetra-pentacene systems reported by Hetzer et al. In that study, the authors compared the transient absorption data to time-resolved EPR experiments collected on their bipentacene species, assigning the three decay components to $^1(T_1T_1)$, $^5(T_1T_1)$, and free T_1.

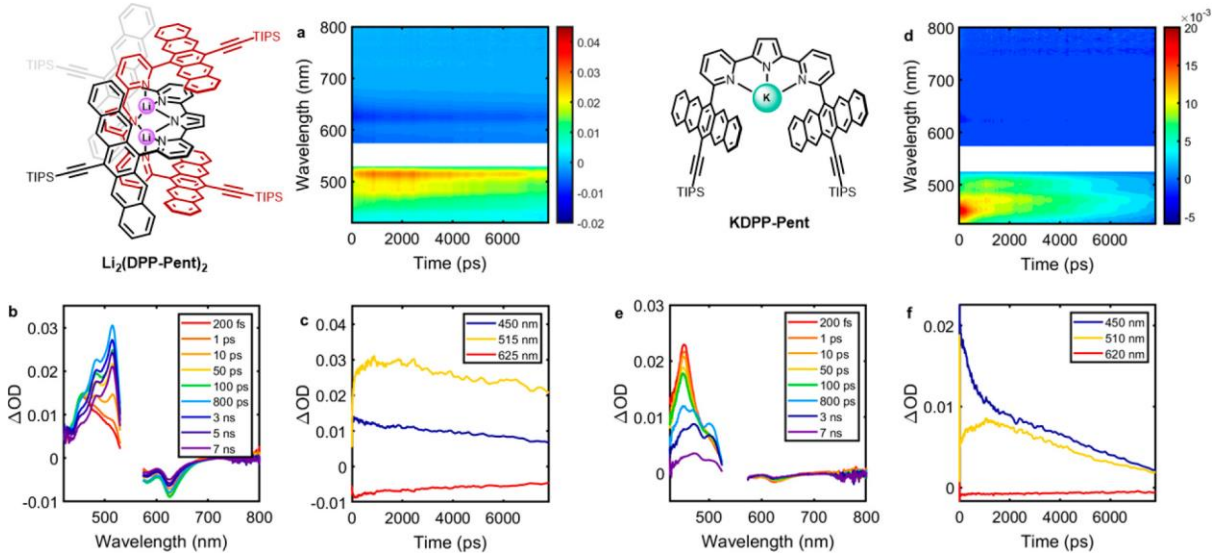

Figure 2.6 Visible transient absorption spectra—Li_2(DPP-Pent)$_2$ and KDPP-Pent. The visible femtosecond transient absorption spectra of Li_2(DPP-Pent)$_2$ and KDPP-Pent (50 μM, toluene) are shown after excitation at 550 nm (0.100 μJ/pulse). Li_2(DPP-Pent)$_2$: (**A**) contour plot, (**B**) spectral traces at various time delays, and (**C**) selected time traces at 450, 515, and 625 nm. KDPP-Pent: (**D**) contour plot, (**E**) spectral traces at various delay times, and (**F**) selected time traces at 450, 510, and 620 nm.

Here, in the absence of additional corroborating evidence, we err on the side of caution and discuss the data in the context of both models. The singlet fission rate is not significantly altered between the two fits. When including a third decay component for the triplet spectral features, though, the fastest triplet lifetime shortens slightly from 23 to 11 ns. In addition, we note that an additional singlet component that decays in parallel to the productive fission pathway could be added to each model; however, the fitted results for each component were not substantially different from the original model, and the rate constants corresponding to the added singlet component had substantially higher standard errors from the fit.

We performed triplet-triplet photosensitization experiments with mixtures of anthracene and Li_2(DPP-Pent)$_2$ in toluene solution, yielding an extinction coefficient for the Li_2(DPP-Pent)$_2$ triplet spectrum at 515 nm of ~52,000 M^{-1} cm^{-1}. We applied this value to the fsTA spectrum after direct excitation at 550 nm gives us an approximate triplet yield of 195%. Ground state bleach analysis via the method of Eaton et al. estimates a triplet yield of 186%.[50] Using these two methods, we place the triplet yield of Li_2(DPP-Pent)$_2$ in the range 186%-195%, considerably higher than in HDPP-Pent.

In the case of KDPP-Pent, the fsTA data show the decay of the ^{1}ESA to a broad feature suggestive of the overlapping singlet and triplet absorption bands observed in HDPP-Pent (Figure

2.5). The nsTA data reveal a structured ^{3}ESA that decays biexponentially. The kinetics could be fitted with both the three-component model applied to the Li_2(DPP-Pent)$_2$ dataset and the four-component model used for HDPP-Pent. There is some absorption intensity in the 400 – 500 nm region in the singular value decomposition of the residual matrix of the three component fit that is adequately accounted for in the four-component model. With regards to the two models, the fittings place a singlet fission time constant in KDPP-Pent around 400 – 600 ps. Despite the qualitative similarity between the K- and HDPP-Pent TA data, little emission intensity was observed from the K complex, and no time-resolved luminescence could be acquired, which suggests that KDPP-Pent may represent an intermediate case between HDPP-Pent and the Li complex.

Comparisons within the DPP-Pent Series

HDPP-Pent undergoes intramolecular singlet fission with a time constant of τ_{SF} of ~730 ps and an estimated 100% triplet yield. Li_2(DPP-Pent)$_2$ is nearly 7-fold faster (τ_{SF} ~ 100 ps) than HDPP-Pent and occurs with higher efficiency (186 – 195% triplet yield). KDPP-Pent, though, demonstrates a rate of singlet fission of 400 – 600 ps, which is similar to HDPP-Pent.

We considered several possibilities for the origin of the rate enhancement observed in Li_2(DPP-Pent)$_2$. First, the NMR data collected on HDPP-Pent demonstrate temperature-dependent conformational dynamics. This suggests that when we excite the solution of HDPP-Pent during the TA experiment, we are exciting a heterogeneity of conformations that are slow to interchange even on the NMR timescale. Some of these conformations may be more or less favorable for intramolecular singlet fission than others, depending on the interpentacene coupling. By deprotonating HDPP-Pent and binding the DPP-Pent moiety to a metal center, we expect the coordination complex to be more rigid than the flexible linker. We posit that this would lead to a

greater uniformity of ground state conformations and could promote greater interactions between the pentacene subunits, leading to more efficient singlet fission. That said, the Li and K complexes both exhibit sharp, well-defined ^{1}H NMR spectra, so structural rigidification alone does not explain the rate enhancement in Li_2(DPP-Pent)$_2$.

Second, the ionic DPP-cation interaction introduces an electric dipole in the vicinity of the pentacene subunits, where a potential Stark effect could influence singlet fission within the system by perturbing the electronic coupling between the relevant excitonic states of the molecule. Li^+ and K^+ have quite different ionic radii (90 and 152 pm, respectively) and we propose there to be two Li^+ cations at the center of the Li_2(DPP-Pent)$_2$ dimer. As a result, we would expect the Li and K complexes to exhibit distinct electric field influences, but at this point it is unclear the extent to which this would differentiate the two.

Third, NMR data supports the assignment of dimeric and monomeric solution-state structures for Li_2(DPP-Pent)$_2$ and KDPP-Pent, respectively. The Li complex exhibits π-stacking interactions between the pentacene rings mediated by a DPP moiety sandwiched in between. Such an π-interaction may enhance the electronic coupling between the two pentacene rings, favoring faster singlet fission. Additionally, the Li dimer brings together four pentacene subunits per molecule as opposed to two (Figure 2.2C). In our proposed structure of Li_2(DPP-Pent)$_2$, the pentacene rings of one DPP-Pent unit are nearly orthogonal to the pentacene rings of the other DPP-Pent unit. This may lead to small overlap between the π-orbitals of the pentacenes, but small structural perturbations or molecular motions could give rise to nonnegligible coupling between the localized states of these pentacenes and impact both singlet fission as well as triplet pair/free triplet distribution over the molecule. We find it likely that this combination of structural

perturbations (including the π-stacking and dimer formation) leads to a pronounced rate enhancement in Li_2(DPP-Pent)$_2$ relative to KDPP-Pent.

Despite the 7-fold rate enhancement in Li_2(DPP-Pent)$_2$, there is little sacrificed in terms of triplet lifetimes. Compared to the ~38 ns and 36 μs lifetimes observed in HDPP-Pent, we find lifetimes of 23 ns and 35 μs in Li_2(DPP-Pent)$_2$ when fitted with a biexponential decay. The faster decay lifetimes in Li_2(DPP-Pent)$_2$ does shorten to 11 ns when fitted to a triexponential, with intermediate and long lifetimes of 100 ns and 50 μs.

Comparison to Previously Reported Bi- and Polypentacenes

In many of the reported bipentacene systems, when there is an increase in the rate of singlet fission, there is also typically an increase in the rate of triplet decay. This has been explained in some bipentacene series by suggesting that the stronger interpentacene electronic coupling that leads to faster singlet fission also simultaneously promotes enhanced triplet-triplet annihilation pathways. The series of phenylene-linked dimers initially reported by Zirzlmeier et al. displays increasing rates of singlet fission going from *meta*- (63 ps) to *para*- (2.7 ps) to *ortho*- (500 fs) and shows a related decrease in triplet pair lifetimes (2.2 ns, 17.3 ps, and 12 ps, respectively). Likewise, the oligophenylene-bridged bipentacenes linked in the 2,2' position reported by Sanders et al. show an analogous increase in singlet fission rate with concomitant reduction in triplet pair lifetimes with decreasing linker units (τ_{SF} from 220 to 20 ps to 760 fs; τ_T from 270 to 16.5 ns to 450 ps for two to one to zero bridging phenylene spacers, respectively). In these cases, conjugated linkers permit strong electronic coupling between pentacenes, which can be modulated via substitution patters on the linker or by increased linker length. Nonconjugated linkers have also been explored, as these systems tend to attenuate the through-bond interpentacene electronic coupling.

Nevertheless, similar trends (increased singlet fission rate with decreased triplet/triplet pair lifetime) have also been observed in such species.

In the DPP-Pent series reported here, the pentacene units are linked in the 6,6'-position by the DPP ligand scaffold. The optimal geometry for the pentacene units is likely orthogonal to the pyridine rings due to steric constraints. In addition to the length of the linking DPP unit, this likely weakens through-bond coupling between the pentacene rings. This is reflected in the relatively slower rate of singlet fission in HDPP-Pent compared to the directly linked *ortho*-, *meta*-, and *para*-phenylene dimers or the oligophenylene-linked systems. In Li_2(DPP-Pent)$_2$, we propose that through-space π-stacking interactions via the intermediary DPP moiety provide an alternative coupling pathway. The rate of singlet fission in Li_2(DPP-Pent)$_2$ (τ_{SF} ~ 100 ps) is still slower than other bipentacenes displaying strong direct pentacene-pentacene π-interactions (typically less than 1 ps) or in the crystalline materials pentacenes are brought in close contact (3 – 4 Å) in the crystal packing. In molecular systems that lack the ability for the triplets to diffuse away from each other, the through-space coupled pentacene dimers tend to have fast triplet pair annihilation pathways, whereas Li_2(DPP-Pent)$_2$ exhibits ns-μs triplet pair/triplet lifetimes.

As previously discussed, the Li complex also has four pentacene units, which could favor a faster rate of singlet fission and slower rate of triplet-triplet annihilation. For example, by comparing adamantyl-linked bi- and tetra-pentacene systems, Hetzer et al. suggested that additional chromophores may effectively delocalize the triplet pair state, providing a favorable entropic factor to the rate of fission. The authors report that the tetra-pentacene species likewise shows very little deviation in the triplet lifetimes from the bipentacene system, despite the faster rate of fission.

The higher-order structure enforced by lithium coordination in Li_2(DPP-Pent)$_2$ likely impacts the photophysics of the system in several ways. First, the through-space π-interactions establish an important coupling pathway that leads to the rate enhancement from HDPP-Pent and KDPP-Pent; however, because the coupling is mediated via the dipyridyl pyrrolide, this interaction is tempered such that the generated triplet pair is longer lived than in other π-stacked bipentacenes. This may work in conjunction with the entropic favorability of having four pentacene rings within a single molecular dimer over which the triplets may diffuse or delocalize.

Conclusion

In summary, we have synthesized the molecular bipentacene system HDPP-Pent that serves as a ligand scaffold. By deprotonation and complexation, we may change the structural morphology and interchromophore interactions in solution in order to effectively tune singlet fission. We propose that the π-stacking interactions and dimeric structure revealed in Li_2(DPP-Pent)$_2$ are critical to its increased singlet fission efficiency compared to the parent HDPP-Pent. This approach highlights the importance of through-space, geometric perturbations that influence singlet fission beyond strict through-bond interactions. Use of coordination chemistry as a means of orienting and controlling excitonic interactions in bipentacene compounds is presented as a new tool for studying singlet fission in molecular systems.

Citations

(1) Smith, M. B.; Michl, J. Singlet Fission. *Chem. Rev.* **2010**, *110* (11), 6891–6936. https://doi.org/10.1021/cr1002613.

(2) Smith, M. B.; Michl, J. Recent Advances in Singlet Fission. *Annual Review of Physical Chemistry* **2013**, *64* (1), 361–386. https://doi.org/10.1146/annurev-physchem-040412-110130.

(3) Swenberg, C. E.; Stacy, W. T. Bimolecular Radiationless Transitions in Crystalline Tetracene. *Chemical Physics Letters* **1968**, *2* (5), 327–328. https://doi.org/10.1016/0009-2614(68)80087-9.

(4) Merrifield, R. E.; Avakian, P.; Groff, R. P. Fission of Singlet Excitons into Pairs of Triplet Excitons in Tetracene Crystals. *Chemical Physics Letters* **1969**, *3* (3), 155–157. https://doi.org/10.1016/0009-2614(69)80122-3.

(5) Merrifield, R. E. Magnetic Effects on Triplet Exciton Interactions. *Pure and Applied Chemistry* **1971**, *27* (3), 481–498. https://doi.org/10.1351/pac197127030481.

(6) Shockley, W.; Queisser, H. J. Detailed Balance Limit of Efficiency of P-n Junction Solar Cells. *Journal of Applied Physics* **1961**, *32* (3), 510–519. https://doi.org/10.1063/1.1736034.

(7) Hanna, M. C.; Nozik, A. J. Solar Conversion Efficiency of Photovoltaic and Photoelectrolysis Cells with Carrier Multiplication Absorbers. *Journal of Applied Physics* **2006**, *100* (7), 074510. https://doi.org/10.1063/1.2356795.

(8) Paci, I.; Johnson, J. C.; Chen, X.; Rana, G.; Popović, D.; David, D. E.; Nozik, A. J.; Ratner, M. A.; Michl, J. Singlet Fission for Dye-Sensitized Solar Cells: Can a Suitable Sensitizer Be Found? *J. Am. Chem. Soc.* **2006**, *128* (51), 16546–16553. https://doi.org/10.1021/ja063980h.

(9) Rao, A.; Wilson, M. W. B.; Hodgkiss, J. M.; Albert-Seifried, S.; Bässler, H.; Friend, R. H. Exciton Fission and Charge Generation via Triplet Excitons in Pentacene/C60 Bilayers. *J. Am. Chem. Soc.* **2010**, *132* (36), 12698–12703. https://doi.org/10.1021/ja1042462.

(10) Ehrler, B.; Wilson, M. W. B.; Rao, A.; Friend, R. H.; Greenham, N. C. Singlet Exciton Fission-Sensitized Infrared Quantum Dot Solar Cells. *Nano Lett.* **2012**, *12* (2), 1053–1057. https://doi.org/10.1021/nl204297u.

(11) Ehrler, B.; Musselman, K. P.; Böhm, M. L.; Friend, R. H.; Greenham, N. C. Hybrid Pentacene/a-Silicon Solar Cells Utilizing Multiple Carrier Generation via Singlet Exciton Fission. *Appl. Phys. Lett.* **2012**, *101* (15), 153507. https://doi.org/10.1063/1.4757612.

(12) Smyser, K. E.; Eaves, J. D. Singlet Fission for Quantum Information and Quantum Computing: The Parallel JDE Model. *Sci Rep* **2020**, *10* (1), 18480. https://doi.org/10.1038/s41598-020-75459-x.

(13) Weiss, L. R.; Bayliss, S. L.; Kraffert, F.; Thorley, K. J.; Anthony, J. E.; Bittl, R.; Friend, R. H.; Rao, A.; Greenham, N. C.; Behrends, J. Strongly Exchange-Coupled Triplet Pairs in an Organic Semiconductor. *Nature Phys* **2017**, *13* (2), 176–181. https://doi.org/10.1038/nphys3908.

(14) Tayebjee, M. J. Y.; Sanders, S. N.; Kumarasamy, E.; Campos, L. M.; Sfeir, M. Y.; McCamey, D. R. Quintet Multiexciton Dynamics in Singlet Fission. *Nature Phys* **2017**, *13* (2), 182–188. https://doi.org/10.1038/nphys3909.

(15) Bayliss, S. L.; Weiss, L. R.; Mitioglu, A.; Galkowski, K.; Yang, Z.; Yunusova, K.; Surrente, A.; Thorley, K. J.; Behrends, J.; Bittl, R.; Anthony, J. E.; Rao, A.; Friend, R. H.; Plochocka, P.; Christianen, P. C. M.; Greenham, N. C.; Chepelianskii, A. D. Site-Selective Measurement of Coupled Spin Pairs in an Organic Semiconductor. *Proceedings of the National Academy of Sciences* **2018**, *115* (20), 5077–5082. https://doi.org/10.1073/pnas.1718868115.

(16) Lubert-Perquel, D.; Salvadori, E.; Dyson, M.; Stavrinou, P. N.; Montis, R.; Nagashima, H.; Kobori, Y.; Heutz, S.; Kay, C. W. M. Identifying Triplet Pathways in Dilute Pentacene Films. *Nat Commun* **2018**, *9* (1), 4222. https://doi.org/10.1038/s41467-018-06330-x.

(17) Wan, Y.; Wiederrecht, G. P.; Schaller, R. D.; Johnson, J. C.; Huang, L. Transport of Spin-Entangled Triplet Excitons Generated by Singlet Fission. *J. Phys. Chem. Lett.* **2018**, *9* (23), 6731–6738. https://doi.org/10.1021/acs.jpclett.8b02944.

(18) Nagashima, H.; Kawaoka, S.; Akimoto, S.; Tachikawa, T.; Matsui, Y.; Ikeda, H.; Kobori, Y. Singlet-Fission-Born Quintet State: Sublevel Selections and Trapping by Multiexciton Thermodynamics. *J. Phys. Chem. Lett.* **2018**, *9* (19), 5855–5861. https://doi.org/10.1021/acs.jpclett.8b02396.

(19) Chen, M.; Krzyaniak, M. D.; Nelson, J. N.; Bae, Y. J.; Harvey, S. M.; Schaller, R. D.; Young, R. M.; Wasielewski, M. R. Quintet-Triplet Mixing Determines the Fate of the Multiexciton State Produced by Singlet Fission in a Terrylenediimide Dimer at Room Temperature. *Proceedings of the National Academy of Sciences* **2019**, *116* (17), 8178–8183. https://doi.org/10.1073/pnas.1820932116.

(20) Matsuda, S.; Oyama, S.; Kobori, Y. Electron Spin Polarization Generated by Transport of Singlet and Quintet Multiexcitons to Spin-Correlated Triplet Pairs during Singlet Fissions. *Chem. Sci.* **2020**, *11* (11), 2934–2942. https://doi.org/10.1039/C9SC04949E.

(21) Hetzer, C.; Guldi, D. M.; Tykwinski, R. R. Pentacene Dimers as a Critical Tool for the Investigation of Intramolecular Singlet Fission. *Chemistry – A European Journal* **2018**, *24* (33), 8245–8257. https://doi.org/10.1002/chem.201705355.

(22) Sanders, S. N.; Pun, A. B.; Parenti, K. R.; Kumarasamy, E.; Yablon, L. M.; Sfeir, M. Y.; Campos, L. M. Understanding the Bound Triplet-Pair State in Singlet Fission. *Chem* **2019**, *5* (8), 1988–2005. https://doi.org/10.1016/j.chempr.2019.05.012.

(23) Korovina, N. V.; Pompetti, N. F.; Johnson, J. C. Lessons from Intramolecular Singlet Fission with Covalently Bound Chromophores. *J. Chem. Phys.* **2020**, *152* (4), 040904. https://doi.org/10.1063/1.5135307.

(24) Wilson, M. W. B.; Rao, A.; Clark, J.; Kumar, R. S. S.; Brida, D.; Cerullo, G.; Friend, R. H. Ultrafast Dynamics of Exciton Fission in Polycrystalline Pentacene. *J. Am. Chem. Soc.* **2011**, *133* (31), 11830–11833. https://doi.org/10.1021/ja201688h.

(25) Rao, A.; Wilson, M. W. B.; Albert-Seifried, S.; Di Pietro, R.; Friend, R. H. Photophysics of Pentacene Thin Films: The Role of Exciton Fission and Heating Effects. *Phys. Rev. B* **2011**, *84* (19), 195411. https://doi.org/10.1103/PhysRevB.84.195411.

(26) Zirzlmeier, J.; Lehnherr, D.; Coto, P. B.; Chernick, E. T.; Casillas, R.; Basel, B. S.; Thoss, M.; Tykwinski, R. R.; Guldi, D. M. Singlet Fission in Pentacene Dimers. *PNAS* **2015**, *112* (17), 5325–5330. https://doi.org/10.1073/pnas.1422436112.

(27) Sanders, S. N.; Kumarasamy, E.; Pun, A. B.; Trinh, M. T.; Choi, B.; Xia, J.; Taffet, E. J.; Low, J. Z.; Miller, J. R.; Roy, X.; Zhu, X.-Y.; Steigerwald, M. L.; Sfeir, M. Y.; Campos, L. M. Quantitative Intramolecular Singlet Fission in Bipentacenes. *J. Am. Chem. Soc.* **2015**, *137* (28), 8965–8972. https://doi.org/10.1021/jacs.5b04986.

(28) Basel, B. S.; Zirzlmeier, J.; Hetzer, C.; Reddy, S. R.; Phelan, B. T.; Krzyaniak, M. D.; Volland, M. K.; Coto, P. B.; Young, R. M.; Clark, T.; Thoss, M.; Tykwinski, R. R.; Wasielewski, M. R.; Guldi, D. M. Evidence for Charge-Transfer Mediation in the Primary Events of Singlet Fission in a Weakly Coupled Pentacene Dimer. *Chem* **2018**, *4* (5), 1092–1111. https://doi.org/10.1016/j.chempr.2018.04.006.

(29) Papadopoulos, I.; Zirzlmeier, J.; Hetzer, C.; Bae, Y. J.; Krzyaniak, M. D.; Wasielewski, M. R.; Clark, T.; Tykwinski, R. R.; Guldi, D. M. Varying the Interpentacene Electronic Coupling to Tune Singlet Fission. *J. Am. Chem. Soc.* **2019**, *141* (15), 6191–6203. https://doi.org/10.1021/jacs.8b09510.

(30) Basel, B. S.; Hetzer, C.; Zirzlmeier, J.; Thiel, D.; Guldi, R.; Hampel, F.; Kahnt, A.; Clark, T.; Guldi, D. M.; Tykwinski, R. R. Davydov Splitting and Singlet Fission in Excitonically Coupled Pentacene Dimers. *Chem. Sci.* **2019**, *10* (13), 3854–3863. https://doi.org/10.1039/C9SC00384C.

(31) Sanders, S. N.; Kumarasamy, E.; Pun, A. B.; Appavoo, K.; Steigerwald, M. L.; Campos, L. M.; Sfeir, M. Y. Exciton Correlations in Intramolecular Singlet Fission. *J. Am. Chem. Soc.* **2016**, *138* (23), 7289–7297. https://doi.org/10.1021/jacs.6b00657.

(32) Sanders, S. N.; Kumarasamy, E.; Pun, A. B.; Steigerwald, M. L.; Sfeir, M. Y.; Campos, L. M. Intramolecular Singlet Fission in Oligoacene Heterodimers. *Angewandte Chemie International Edition* **2016**, *55* (10), 3373–3377. https://doi.org/10.1002/anie.201510632.

(33) Fuemmeler, E. G.; Sanders, S. N.; Pun, A. B.; Kumarasamy, E.; Zeng, T.; Miyata, K.; Steigerwald, M. L.; Zhu, X.-Y.; Sfeir, M. Y.; Campos, L. M.; Ananth, N. A Direct Mechanism of Ultrafast Intramolecular Singlet Fission in Pentacene Dimers. *ACS Cent. Sci.* **2016**, *2* (5), 316–324. https://doi.org/10.1021/acscentsci.6b00063.

(34) Kumarasamy, E.; Sanders, S. N.; Tayebjee, M. J. Y.; Asadpoordarvish, A.; Hele, T. J. H.; Fuemmeler, E. G.; Pun, A. B.; Yablon, L. M.; Low, J. Z.; Paley, D. W.; Dean, J. C.; Choi, B.; Scholes, G. D.; Steigerwald, M. L.; Ananth, N.; McCamey, D. R.; Sfeir, M. Y.; Campos, L. M. Tuning Singlet Fission in π-Bridge-π Chromophores. *J. Am. Chem. Soc.* **2017**, *139* (36), 12488–12494. https://doi.org/10.1021/jacs.7b05204.

(35) Mandal, A.; Chen, M.; Foszcz, E. D.; Schultz, J. D.; Kearns, N. M.; Young, R. M.; Zanni, M. T.; Wasielewski, M. R. Two-Dimensional Electronic Spectroscopy Reveals Excitation Energy-Dependent State Mixing during Singlet Fission in a Terrylenediimide Dimer. *J. Am. Chem. Soc.* **2018**, *140* (51), 17907–17914. https://doi.org/10.1021/jacs.8b08627.

(36) Hetzer, C.; Basel, B. S.; Kopp, S. M.; Hampel, F.; White, F. J.; Clark, T.; Guldi, D. M.; Tykwinski, R. R. Chromophore Multiplication To Enable Exciton Delocalization and Triplet

Diffusion Following Singlet Fission in Tetrameric Pentacene. *Angewandte Chemie International Edition* **2019**, *58* (43), 15263–15267. https://doi.org/10.1002/anie.201907221.

(37) Casillas, R.; Adam, M.; Coto, P. B.; Waterloo, A. R.; Zirzlmeier, J.; Reddy, S. R.; Hampel, F.; McDonald, R.; Tykwinski, R. R.; Thoss, M.; Guldi, D. M. Intermolecular Singlet Fission in Unsymmetrical Derivatives of Pentacene in Solution. *Advanced Energy Materials* **2019**, *9* (2), 1802221. https://doi.org/10.1002/aenm.201802221.

(38) Basel, B. S.; Young, R. M.; Krzyaniak, M. D.; Papadopoulos, I.; Hetzer, C.; Gao, Y.; Porte, N. T. L.; Phelan, B. T.; Clark, T.; Tykwinski, R. R.; Wasielewski, M. R.; Guldi, D. M. Influence of the Heavy-Atom Effect on Singlet Fission: A Study of Platinum-Bridged Pentacene Dimers. *Chem. Sci.* **2019**, *10* (48), 11130–11140. https://doi.org/10.1039/C9SC04410H.

(39) Papadopoulos, I.; Gao, Y.; Hetzer, C.; Tykwinski, R. R.; Guldi, D. M. Singlet Fission in Enantiomerically Pure Pentacene Dimers. *ChemPhotoChem* **2020**, *4* (10), 5168–5174. https://doi.org/10.1002/cptc.202000016.

(40) Chen, M.; Bae, Y. J.; Mauck, C. M.; Mandal, A.; Young, R. M.; Wasielewski, M. R. Singlet Fission in Covalent Terrylenediimide Dimers: Probing the Nature of the Multiexciton State Using Femtosecond Mid-Infrared Spectroscopy. *J. Am. Chem. Soc.* **2018**, *140* (29), 9184–9192. https://doi.org/10.1021/jacs.8b04830.

(41) Zirzlmeier, J.; Casillas, R.; Reddy, S. R.; Coto, P. B.; Lehnherr, D.; Chernick, E. T.; Papadopoulos, I.; Thoss, M.; Tykwinski, R. R.; Guldi, D. M. Solution-Based Intramolecular Singlet Fission in Cross-Conjugated Pentacene Dimers. *Nanoscale* **2016**, *8* (19), 10113–10123. https://doi.org/10.1039/C6NR02493A.

(42) Shetty, A. S.; Zhang, J.; Moore, J. S. Aromatic π-Stacking in Solution as Revealed through the Aggregation of Phenylacetylene Macrocycles. *J. Am. Chem. Soc.* **1996**, *118* (5), 1019–1027. https://doi.org/10.1021/ja9528893.

(43) Platts, J. A.; Gkionis, K. NMR Shielding as a Probe of Intermolecular Interactions: Ab Initio and Density Functional Theory Studies. *Phys. Chem. Chem. Phys.* **2009**, *11* (44), 10331–10339. https://doi.org/10.1039/B822560E.

(44) Bothner-By, A. A.; Stephens, R. L.; Lee, J.; Warren, C. D.; Jeanloz, R. W. Structure Determination of a Tetrasaccharide: Transient Nuclear Overhauser Effects in the Rotating Frame. *J. Am. Chem. Soc.* **1984**, *106* (3), 811–813. https://doi.org/10.1021/ja00315a069.

(45) Bax, A.; Davis, D. G. Practical Aspects of Two-Dimensional Transverse NOE Spectroscopy. *Journal of Magnetic Resonance (1969)* **1985**, *63* (1), 207–213. https://doi.org/10.1016/0022-2364(85)90171-4.

(46) Walker, B. J.; Musser, A. J.; Beljonne, D.; Friend, R. H. Singlet Exciton Fission in Solution. *Nature Chem* **2013**, *5* (12), 1019–1024. https://doi.org/10.1038/nchem.1801.

(47) Bensasson, R.; Land, E. J. Triplet-Triplet Extinction Coefficients via Energy Transfer. *Trans. Faraday Soc.* **1971**, *67* (0), 1904–1915. https://doi.org/10.1039/TF9716701904.

(48) Compton, R. H.; Grattan, K. T. V.; Morrow, T. Extinction Coefficients and Quantum Yields for Triplet—Triplet Absorption Using Laser Flash Photolysis. *Journal of Photochemistry* **1980**, *14* (1), 61–66. https://doi.org/10.1016/0047-2670(80)85068-4.

(49) Nielsen, B. R.; Jørgensen, K.; Skibsted, L. H. Triplet—Triplet Extinction Coefficients, Rate Constants of Triplet Decay and Rate Constant of Anthracene Triplet Sensitization by Laser Flash Photolysis of Astaxanthin, β-Carotene, Canthaxanthin and Zeaxanthin in Deaerated Toluene at 298 K. *Journal of Photochemistry and Photobiology A: Chemistry* **1998**, *112* (2), 127–133. https://doi.org/10.1016/S1010-6030(97)00285-2.

(50) Eaton, S. W.; Shoer, L. E.; Karlen, S. D.; Dyar, S. M.; Margulies, E. A.; Veldkamp, B. S.; Ramanan, C.; Hartzler, D. A.; Savikhin, S.; Marks, T. J.; Wasielewski, M. R. Singlet Exciton Fission in Polycrystalline Thin Films of a Slip-Stacked Perylenediimide. *J. Am. Chem. Soc.* **2013**, *135* (39), 14701–14712. https://doi.org/10.1021/ja4053174.